

This article was downloaded by:[Bochkarev, N.]  
On: 12 December 2007  
Access Details: [subscription number 746126554]  
Publisher: Taylor & Francis  
Informa Ltd Registered in England and Wales Registered Number: 1072954  
Registered office: Mortimer House, 37-41 Mortimer Street, London W1T 3JH, UK



# Astronomical & Astrophysical Transactions

## The Journal of the Eurasian Astronomical Society

Publication details, including instructions for authors and subscription information:  
<http://www.informaworld.com/smpp/title~content=t713453505>

### Gasodynamical model of the triaxial protogalaxy collapse

P. Berczik<sup>a</sup>; I. G. Kolesnik<sup>a</sup>

<sup>a</sup> Main Astronomical Observatory of Ukrainian National Academy of Sciences, Golosiiv, Ukraine

Online Publication Date: 01 May 1998

To cite this Article: Berczik, P. and Kolesnik, I. G. (1998) 'Gasodynamical model of the triaxial protogalaxy collapse', *Astronomical & Astrophysical Transactions*, 16:3, 163 - 185

To link to this article: DOI: 10.1080/10556799808208155

URL: <http://dx.doi.org/10.1080/10556799808208155>

PLEASE SCROLL DOWN FOR ARTICLE

Full terms and conditions of use: <http://www.informaworld.com/terms-and-conditions-of-access.pdf>

This article maybe used for research, teaching and private study purposes. Any substantial or systematic reproduction, re-distribution, re-selling, loan or sub-licensing, systematic supply or distribution in any form to anyone is expressly forbidden.

The publisher does not give any warranty express or implied or make any representation that the contents will be complete or accurate or up to date. The accuracy of any instructions, formulae and drug doses should be independently verified with primary sources. The publisher shall not be liable for any loss, actions, claims, proceedings, demand or costs or damages whatsoever or howsoever caused arising directly or indirectly in connection with or arising out of the use of this material.

# GASODYNAMICAL MODEL OF THE TRIAXIAL PROTOGALAXY COLLAPSE

P. BERCZIK and I. G. KOLESNIK

*Main Astronomical Observatory of Ukrainian National Academy of Sciences,  
252650, Golosiiv, Kiev-022, Ukraine*

*(Received February 14, 1996)*

This is the first article in a series of papers about the 3D models of triaxial galaxy formation carried out by the Smoothed Particle Hydrodynamics (SPH) method (Berczik and Kolesnik, 1993, 1995). We use the triaxial model for initial conditions of protogalaxies. We model the body of protogalaxies by triaxial ellipsoids with semiaxes  $A, B$  and  $C$ . Initial velocity fields are defined by the initial angular velocity  $\Omega_0$ . The total angular momentum does not coincide with semiaxes. Therefore the initial velocity field can be described by the formula:  $V_0(x, y, z) = [\Omega_0 \times r]$ . In this paper we discuss a series of models of an isothermal and adiabatic collapse of pure gas triaxial protogalaxies.

KEY WORDS Galactic formation, SPH, triaxial galaxies, warp galactic structures

## 1 INTRODUCTION

We not discuss here in detail the process that lead to a formation of a triaxial protogalaxy. This is an independent cosmological problem that needs a separate investigation. But, as we know, the protogalactic perturbation in the early universe may be triaxial (Berdeen *et al.*, 1986; White and Silk, 1979; Eisenstein and Loeb, 1995). Therefore, when the galaxy is formed through the evolution of a triaxial protogalaxy fragment, the resulting galaxy also may be triaxial.

The problem of the origin of the initial angular momentum of a protogalaxy have many different solutions (Voglis and Hiotelis, 1989; Chernin, 1993). But, in common cases, the models shows that there exists a probability that the protogalaxy has on initial total angular momentum vector which does not coincide with any of the main axes of the triaxial initial protogalactic figure. Then, as a result of a dynamical collapse, we can expect a triaxial galaxy having complicated internal kinematics (Curir and Diaferio, 1994).

The number of data on galaxies being triaxial in their majority increases steadily. First of all, elliptical galaxies are triaxial (Illingworth, 1977; Binney, 1978, 1985). This conclusion, in many cases, follows from the analysis of the shape and brightness distribution of the images of elliptical galaxies. Still more convincing data on

the triaxial shape of ellipticals are obtained from their kinematical properties. New investigations confirm this idea, and now we may make a conclusion that all ellipticals are triaxial (Franx *et al.*, 1989; Kormendy and Djorgovski, 1989; de Zeeuw and Franx, 1991; Franx *et al.*, 1991).

It is also possible for the warping processes in the disk system to be examined as an evidence of the general triaxiality of this system (Binney, 1992). Asymmetries in the distribution of light and neutral hydrogen are also often observed in disk galaxies (Richter and Sancisi, 1994). On the basis of the data about bar – galaxies we conclude that a considerable part of such systems has an essentially triaxial gravitational potential (Pfenniger, 1984). Now the number of data about the triaxiality of bulges in spiral galaxies steadily increases (Bertola *et al.*, 1991; Weinberg, 1992). The Milkyway galaxy and M31 also may have extended triaxial bulges (Blitz and Spergel, 1991a,b).

Really, there exist some various processes that can lead to a formation of triaxial galaxies, e.g. “cold” nondissipative collapse of spherical systems (Aguilar and Merritt, 1990; Voglis, 1994). But a great number of triaxial shaping among the galaxies generates an idea that triaxial configuration can initially exist on the protogalactic stage of evolution. We expect that this triaxial form already exists on the early state of evolution of protogalaxies, when the star formation does still not start, and protogalaxies have only pure gas components. From our point of view, the triaxiality of protogalaxies may be the main generating factor of the present triaxial shape of galaxies.

In this paper we consider a case, when in the initial state the protogalaxy is a homogeneous triaxial ellipsoid having an angular momentum arbitrary oriented in space. Simulations were carried out by the SPH method. The properties of early gas galaxies, which can be formed as a result of an isothermal or adiabatic collapse, are considered.

In the next paper, we shall describe the result of the next series of models, in which we shall include the star formation process in the evolution of a triaxial protogalaxy.

## 2 THE SPH CODE FOR SIMULATIONS OF GALAXY FORMATION

### 2.1 Basic Principles

Continuous hydrodynamic fields in SPH are described by the interpolation functions constructed from the known values of these functions at randomly positioned particles. In this case the mean value of a physical field  $f(\mathbf{r})$  at the point  $\mathbf{r}$  can be written as (Monaghan, 1992; Monaghan and Lattanzio, 1985):

$$\langle f(\mathbf{r}) \rangle = \int f(\mathbf{r}') \cdot W(\mathbf{r} - \mathbf{r}'; h) d\mathbf{r}', \quad (1)$$

where  $W(\mathbf{r} - \mathbf{r}'; h)$  is the kernel function and  $h$  is the softening constant.

The function  $W(\mathbf{u}; h)$  is strongly peaked at  $|\mathbf{u}| = 0$ , and we can consider it without any loss of generality as belonging to the class of even functions. In this case it is not difficult to demonstrate (Hernquist and Katz, 1989) that the average value  $\langle f(\mathbf{r}) \rangle$  represents the real function  $f(\mathbf{r})$ , with an error not higher than  $O(h^2)$ :

Consider a fluid with the density  $\rho(\mathbf{r})$ . We rewrite (1) in the form

$$\langle f(\mathbf{r}) \rangle = \int \frac{f(\mathbf{r}')}{\rho(\mathbf{r}')} \cdot W(\mathbf{r} - \mathbf{r}'; h) \cdot \rho(\mathbf{r}') d\mathbf{r}'. \quad (2)$$

Let us imagine that  $f(\mathbf{r})$  and  $\rho(\mathbf{r})$  are known only at  $N$  discrete points  $\mathbf{r}_i$ . Then, equation (2) gives

$$f_i = \sum_{j=1}^N m_j \cdot \frac{f_j}{\rho_j} \cdot W_{ij}. \quad (3)$$

Here  $f_i \equiv f(\mathbf{r}_i)$ ,  $\rho_i \equiv \rho(\mathbf{r}_i)$ ,  $W_{ij} \equiv W(\mathbf{r}_i - \mathbf{r}_j; h)$  and  $m_i$  is a mass of particle  $i$ .

Using (3), we approximate the hydrodynamic field by an analytical function which is differentiable as many times as the kernel  $W_{ij}$ .

Following Monaghan and Lattanzio (1985) for the kernel function  $W_{ij}$  we shall use the spline expression in the form

$$W_{ij} = \frac{1}{\pi h^3} \begin{cases} 1 - \frac{3}{2} \left(\frac{u_{ij}}{h}\right)^2 + \frac{3}{4} \left(\frac{u_{ij}}{h}\right)^3, & \text{if } 0 \leq \frac{u_{ij}}{h} \leq 1; \\ \frac{1}{4} \left(2 - \frac{u_{ij}}{h}\right)^3, & \text{if } 1 \leq \frac{u_{ij}}{h} \leq 2; \\ 0, & \text{otherwise.} \end{cases} \quad (4)$$

The local resolution in SPH is defined by the chosen smoothing length  $h$ . If it is the same for all points, the hydrodynamic field will be evidently approximated more smoothly in the regions where the points lie more closely; i.e. where the density is higher.

To achieve the same level of accuracy for all points in the fluid, it is necessary to use a spatially variable smoothing length. In this case each particle has its individual value of  $h$ . Following Hernquist and Katz (1989), instead of (1) we shall write

$$\langle f(\mathbf{r}) \rangle = \int f(\mathbf{r}') \cdot \frac{1}{2} \cdot [W(\delta\mathbf{r}; h) + W(\delta\mathbf{r}; h')] d\mathbf{r}'. \quad (5)$$

Here  $\delta\mathbf{r} \equiv \mathbf{r} - \mathbf{r}'$ ,  $h \equiv h(\mathbf{r})$  and  $h' \equiv h(\mathbf{r}')$ . For the density  $\rho(\mathbf{r})$  it gives

$$\langle \rho(\mathbf{r}_i) \rangle = \sum_{j=1}^N m_j \cdot \frac{1}{2} \cdot [W(r_{ij}; h_i) + W(r_{ij}; h_j)]. \quad (6)$$

Other hydrodynamic functions are written in the same manner.

Many different procedures were proposed for choosing of individual smoothing lengths  $h_i$ . In our calculations the values of  $h_i$  were determined from the condition that the number of particles  $N_B$  in the neighbourhood of each particle remains constant. The value of  $N_B$  is chosen such that a certain fraction from the total number of particles  $N$  affects the local flow characteristics (Hiotelis and Voglis, 1991).

## 2.2 Hydrodynamics Equations

If the density is computed according to the equation (6), then the continuity equation is satisfied automatically. The equations of motion for particle  $i$  are

$$\frac{d\mathbf{r}_i}{dt} = \mathbf{v}_i, \quad (7)$$

$$\frac{d\mathbf{v}_i}{dt} = -\frac{\nabla_i P_i}{\rho_i} + \mathbf{a}_i^{\text{vis}} - \nabla_i \Phi_i, \quad (8)$$

where  $P_i$  is the pressure,  $\Phi_i$  is the gravitational potential,  $\mathbf{a}_i^{\text{vis}}$  is an artificial viscosity term. Using the equations (5) and (6) we can write:

$$\frac{\nabla_i P_i}{\rho_i} = \sum_{j=1}^N m_j \cdot \frac{1}{2} \cdot \left( \frac{P_i}{\rho_i^2} + \frac{P_j}{\rho_j^2} \right) \times [\nabla_i W(r_{ij}; h_i) + \nabla_i W(r_{ij}; h_j)]. \quad (9)$$

The artificial viscosity term  $\mathbf{a}_i^{\text{vis}}$  is introduced to describe flows with shock waves. In present calculations the viscous acceleration was introduced by replacing  $(P_i/\rho_i^2 + P_j/\rho_j^2)$  in equation (9) by  $(P_i/\rho_i^2 + P_j/\rho_j^2) \cdot (1 + \pi_{ij})$ . The expression for  $\pi_{ij}$  has the form (Hietelis *et al.*, 1991)

$$\pi_{ij} = -\alpha \cdot \mu_{ij} + \beta \cdot \mu_{ij}^2, \quad (10)$$

where  $\alpha$  and  $\beta$  are constants, and  $\mu_{ij}$  is defined by the relation

$$\mu_{ij} = \begin{cases} \frac{h_{ij}(\mathbf{v}_{ij} \cdot \mathbf{r}_{ij})}{c_{ij}(r_{ij}^2 + n^2 \cdot h_{ij}^2)}, & \text{if } (\mathbf{v}_{ij} \cdot \mathbf{r}_{ij}) < 0; \\ 0, & \text{otherwise.} \end{cases} \quad (11)$$

Here  $c_{ij} = (c_i + c_j)/2$  is the sound speed averaged for points  $i$  and  $j$ ;  $h_{ij} = (h_i + h_j)/2$ ;  $\mathbf{r}_{ij} = (\mathbf{r}_i - \mathbf{r}_j)$  and  $\mathbf{v}_{ij} = (\mathbf{v}_i - \mathbf{v}_j)$  is the relative velocity vector for the points  $i$  and  $j$ . The term  $n^2 \cdot h_{ij}^2$  is inserted to prevent divergences when  $r_{ij} = 0$  and it should be small enough. The constant  $n$  was set equal to 0.1. For the constant  $\alpha$  and  $\beta$  in (10) the values  $\alpha = 1$  and  $\beta = 2$  give good results in a wide range of the Mach numbers (Monaghan, 1992).

By using equation (4), for the gravitational acceleration  $-\nabla_i \Phi_i$  one gets (Hietelis and Voglis, 1991)

$$-\nabla_i \Phi_i = -\frac{1}{2} \cdot \sum_{j=1}^N G \cdot m_j \cdot \frac{\mathbf{r}_{ij}}{r_{ij}^3} \cdot [g(u_i) + g(u_j)], \quad (12)$$

where

$$g(u_k) = \begin{cases} \frac{4}{3} \cdot u_k^3 - \frac{6}{5} \cdot u_k^5 + \frac{1}{2} \cdot u_k^6, & \text{if } 0 \leq u_k \leq 1; \\ -\frac{1}{15} + \frac{8}{3} u_k^3 - 3u_k^4 + \frac{6}{5} u_k^5 - \frac{1}{6} u_k^6, & \text{if } 1 \leq u_k \leq 2; \\ 1, & \text{otherwise.} \end{cases}$$

and  $u_k = \frac{r_{ij}}{h_k}$ .

When isothermal flows are considered, the system of equations is closed by adding the equation of state:

$$P_i = \rho_i \cdot c_i^2, \quad (13)$$

where  $c_i$  is the isothermal speed of sound.

For adiabatic flows the energy equation in the particle representation has the form

$$\begin{aligned} \frac{du_i}{dt} &= \sum_{j=1}^N m_j \cdot \frac{1}{4} \cdot \left( \frac{P_i}{\rho_i^2} + \frac{P_j}{\rho_j^2} \right) \cdot (1 + \pi_{ij}) \\ &\times [\nabla_i W(r_{ij}; h_i) + \nabla_j W(r_{ij}; h_j)] \cdot u_{ij} \end{aligned} \quad (14)$$

where  $u_i$  is the specific internal energy of particle  $i$ . And to close the system, the equation of state must be added, which can be written in the form

$$P_i = \rho_i \cdot (\gamma - 1) \cdot u_i, \quad (15)$$

where  $\gamma$  is the adiabatic index.

### 2.3 The SPH Code

To solve the system of equations (7), (8) and (14) we use the algorithm of individual time steps. This system of equations has the form

$$\begin{cases} d\mathbf{r}_i/dt = \mathbf{v}_i; \\ d\mathbf{v}_i/dt = \mathbf{F}_i(P, \rho, \mathbf{r}, \mathbf{v}); \\ du_i/dt = G_i(P, \rho, \mathbf{r}, \mathbf{v}). \end{cases} \quad (16)$$

The time step  $\delta t_i$  for each particle depends on the particle's acceleration  $a_i$ , and velocity  $\mathbf{v}_i$ , as well on viscous forces.

To define  $\delta t_i$  we will use the relation (Hiotelis and Voglis, 1991)

$$\delta t_i = C_n \min \left[ \left( \frac{h_i}{|a_i|} \right)^{1/2}, \frac{h_i}{|\mathbf{v}_i|}, \frac{h_i}{s_i} \right], \quad (17)$$

where  $s_i = c_i \cdot (1 + \alpha + 0.68 \cdot \beta \cdot \max |\mu_{ij}|)$  and  $C_n$  is Courant's number. Usually  $C_n = 0.01 \div 0.1$ .

The system of equations (16) is integrated in five steps.

*Step one.* Let  $t_i$  and  $\delta t_i$  be the current time and time step for  $i$ th particle. We choose such a particle  $i_*$  that have the minimum value of  $t_i + \delta t_i$ . For this particle  $t_* = t_{i_*}$ ,  $\delta t_* = \delta t_{i_*}$ . Thereafter we find for other particles

$$\delta t_i^{(1/2)} = \frac{1}{2} \cdot \delta t_* + (t_* - t_i),$$

and

$$\delta t_i^{(1)} = \delta t_* + (t_* - t_i).$$

*Step two.* Using the Euler method ( $y_{n+1} - y_n = \Delta x \cdot f(x, y_n)$ ), we predict the values of  $\mathbf{r}_i^{(n+1/2)}$ ,  $\mathbf{v}_i^{(n+1/2)}$ ,  $u_i^{(n+1/2)}$  and  $\rho_i^{(n+1/2)}$  for all particles at the moment  $t = t_i + \delta t_i^{(1/2)}$ . To obtain  $\rho_i^{(n+1/2)}$  for all particles except  $i_*$ , we use equation (6) in which only  $\mathbf{r}_{ij}$  varies with time. The calculation relations are

$$\begin{cases} \mathbf{r}_i^{(n+1/2)} = \mathbf{r}_i^{(n)} + \delta t_i^{(1/2)} \cdot \mathbf{v}_i^{(n)}; \\ \mathbf{v}_i^{(n+1/2)} = \mathbf{v}_i^{(n)} + \delta t_i^{(1/2)} \cdot \mathbf{F}_i^{(n)}(P, \rho, \mathbf{r}, \mathbf{v}); \\ u_i^{(n+1/2)} = u_i^{(n)} + \delta t_i^{(1/2)} \cdot G_i^{(n)}(P, \rho, \mathbf{r}, \mathbf{v}); \\ \rho_i^{(n+1/2)} = \rho_i^{(n)} + \delta t_i^{(1/2)} \times \sum_{j=1}^n m_j \frac{1}{2} [\dot{W}(r_{ij}; h_i) + \dot{W}(r_{ij}; h_j)], \end{cases} \quad (18)$$

where

$$\dot{W}(r_{ij}; h) = \frac{1}{\pi h^3} \begin{cases} \frac{3}{4} \frac{\mathbf{v}_{ij} \mathbf{r}_{ij}}{h^2} (3 \frac{r_{ij}}{h} - 4), & \text{if } 0 \leq \frac{r_{ij}}{h} \leq 1; \\ -\frac{3}{4} \frac{\mathbf{v}_{ij} \mathbf{r}_{ij}}{h r_{ij}} (2 - \frac{r_{ij}}{h})^2, & \text{if } 1 \leq \frac{r_{ij}}{h} \leq 2; \\ 0, & \text{otherwise.} \end{cases}$$

The values thus obtained need not be stored in separate arrays, they are used only for exact integration of the equation for the particle  $i_*$ .

*Step three.* The density  $\rho_*$  is most sensitive to time variations on the interval  $\delta t_*$ . Therefore, we firstly, by the quicksort algorithm, find a new value of  $h_*^{(n+1/2)}$  based on the predicted values of  $\mathbf{r}_i^{(n+1/2)}$  and then determine  $\rho_*^{(n+1/2)}$  from the exact equation (6). This value of density is used to calculate the particle  $i_*$  parameters for the moment  $t_* + \frac{1}{2} \cdot \delta t_*$  from equations (18).

*Step four.* We find the particle  $i_*$  parameters at the moment  $t_* + \delta t_*$ :

$$\begin{cases} \mathbf{v}_*^{(n+1)} = \mathbf{v}_*^{(n)} + \delta t_* \cdot \mathbf{F}_*^{(n+1/2)}(P, \rho, \mathbf{r}, \mathbf{v}); \\ \mathbf{r}_*^{(n+1)} = \mathbf{r}_*^{(n)} + \delta t_* \cdot \frac{1}{2} \cdot (\mathbf{v}_*^{(n)} + \mathbf{v}_*^{(n+1)}); \\ u_*^{(n+1)} = u_*^{(n)} + \delta t_* \cdot G_*^{(n+1/2)}(P, \rho, \mathbf{r}, \mathbf{v}). \end{cases} \quad (19)$$

*Step five.* Substituting  $\delta t_i^{(1)}$  instead of  $\delta t_*^{(1/2)}$  in (18), we synchronize the parameters for all particles except  $i_*$  at the moment  $t_* + \delta t_*$ . Thereafter we define the new value of  $h_*^{(n+1)}$  based on the values  $\mathbf{r}_i^{(n+1)}$  and find  $\rho_*^{(n+1)}$  using equation (6). After that the current time is set equal to  $t_* + \delta t_*$ . The new time step for  $\delta t_i$  is determined, and all cycle is repeated.

We have carried out (Berczik and Kolesnik, 1993) a large series of test calculations to check that the code elaborated is correct, the conservation laws are obeyed and the hydrodynamic fields are represented adequately. These tests have shown good results.

### 3 OVERVIEW OF MODELS

#### 3.1 Initial Conditions

We suppose, the common initial conditions for protogalaxy. We model the initial body of protogalaxy by homogenous triaxial  $HI$  ellipsoids with semiaxes  $A$ ,  $B$  and

$C$ . In all models we take  $M_{HI} = 10^{12} M_{\odot}$  as the mass of protogalaxy. We take the initial temperature of gas  $T_0$ . The initial orientation of ellipsoid semiaxes  $A$ ,  $B$  and  $C$  coincides with the axes of the coordinate system  $(x, y, z)$ . The initial velocity fields are defined through the angular velocity  $\Omega_0(x, y, z)$ .

$$V_0(x, y, z) = [\Omega_0(x, y, z) \times \mathbf{r}].$$

The initial angular velocity  $\Omega_0$  is taken constant in space. Therefore  $\Omega_0(x, y, z) \equiv \Omega_0 = \text{Const}$ . The orientation of the initial angular velocity is defined by its components:  $(\Omega_{0x}, \Omega_{0y}, \Omega_{0z})$ . We investigate a different orientation of the initial angular velocity. The standard spin parameter defined as (Peebles, 1969):

$$\lambda = \frac{|L_0| \cdot \sqrt{|E_0^{gr}|}}{G \cdot M_{HI}^{5/2}} \tag{20}$$

where the  $L_0$  is the total initial angular momentum and the  $E_0^{gr}$  is the total initial gravitational energy of a protogalaxy.

In all models we carry out two series of the calculations with  $N = 515$  and  $N = 4169$  gas particles. We take the parameter  $N_B$  equal to 5 for the first series of models and to 10 for the second series of models. We take the initial centre of particles in space with an equal step for the three coordinate axes. Therefore the initial configuration of particles forms a system of homogenous cubic cells. The Table 1 lists parameters of models. The  $\Omega_{\text{cir}} = V_{\text{cir}}/A$  and  $V_{\text{cir}} = (G \cdot M_{HI}/A)^{1/2}$ . The  $A$ ,  $B$  and  $C$ , in the Table 1, are shown in kpc.

**Table 1.** The list of parameters

$A$	$B$	$C$	$\Omega_0/\Omega_{\text{cir}}$	$\lambda$	$T_0 = 10^4$	$10^5$	$5 \times 10^5$	$10^4$ ( <i>adiab</i> )
100	90	50	(0.8, 0.0, 0.8)	0.28	-	-	B1	-
100	60	50	(0.5, 0.0, 0.5)	0.13	-	-	T1	-
100	75	50	(0.8, 0.0, 0.8)	0.21	-	TT1	-	-
100	75	50	(0.5, 0.0, 0.5)	0.13	-	-	-	TT1A
100	75	50	(0.8, 0.0, 0.4)	0.11	TT2	-	-	-
100	75	50	(0.4, 0.0, 0.8)	0.22	TT4	-	-	-

In the case when the angular momentum was acquired by the tidal torque of the matter around the protogalaxy, spin parameter does not exceed  $\lambda \approx 0.1$  (Voglis and Hiotelis, 1989; Zurek *et al.*, 1988; Eisenstein and Loeb, 1995). In our calculations we investigate the case when the protogalaxy may also have an additional own angular momentum of the order or more than the angular momentum defined by the tidal torque. As a result, we take the value of the initial spin parameter of the protogalaxy to be  $\lambda \approx 0.1 \div 0.3$ .

### 3.2 Discussion of the Results

The global evolution of isothermal models in the second series B1, T1, TT1 and the adiabatic model TT1A are shown in Figures 1, 2, 3 and 4.



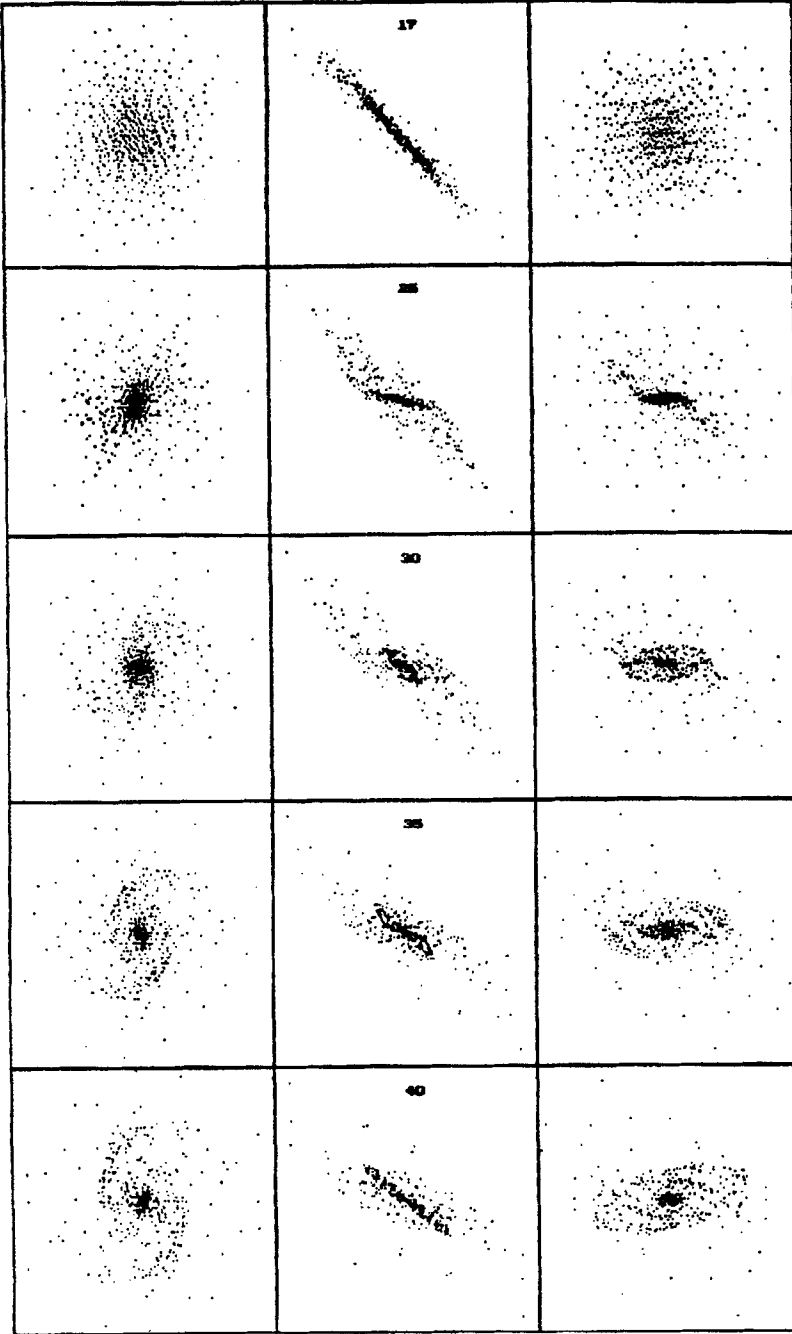


Figure 1 The model B1. The first column correspond to XY plane; the second, XZ plane and the third, YZ plane. The step 17 corresponds to  $t \approx 0.61 \times 10^9$  year. The step 40 corresponds to  $t \approx 0.98 \times 10^9$  year. The diameter of cell represented in the figure is 200 kpc.

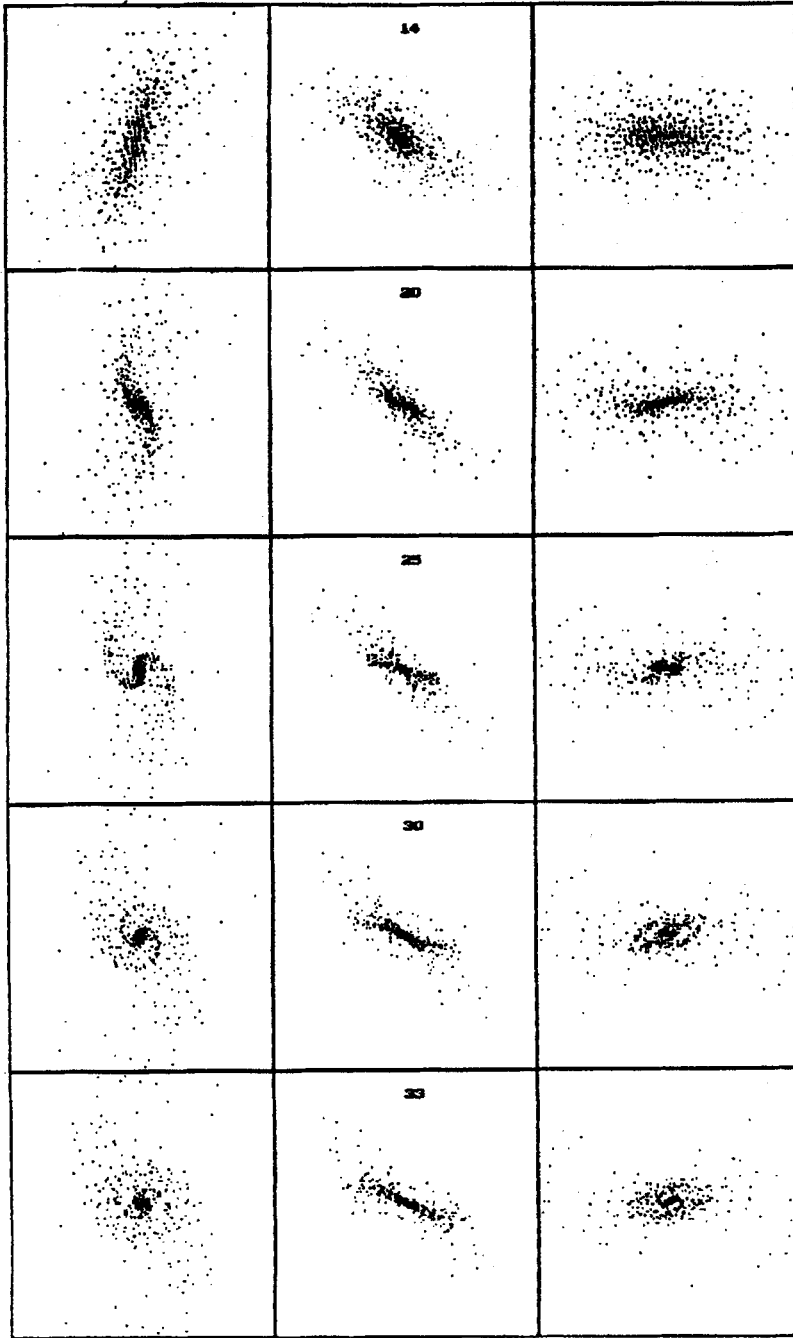
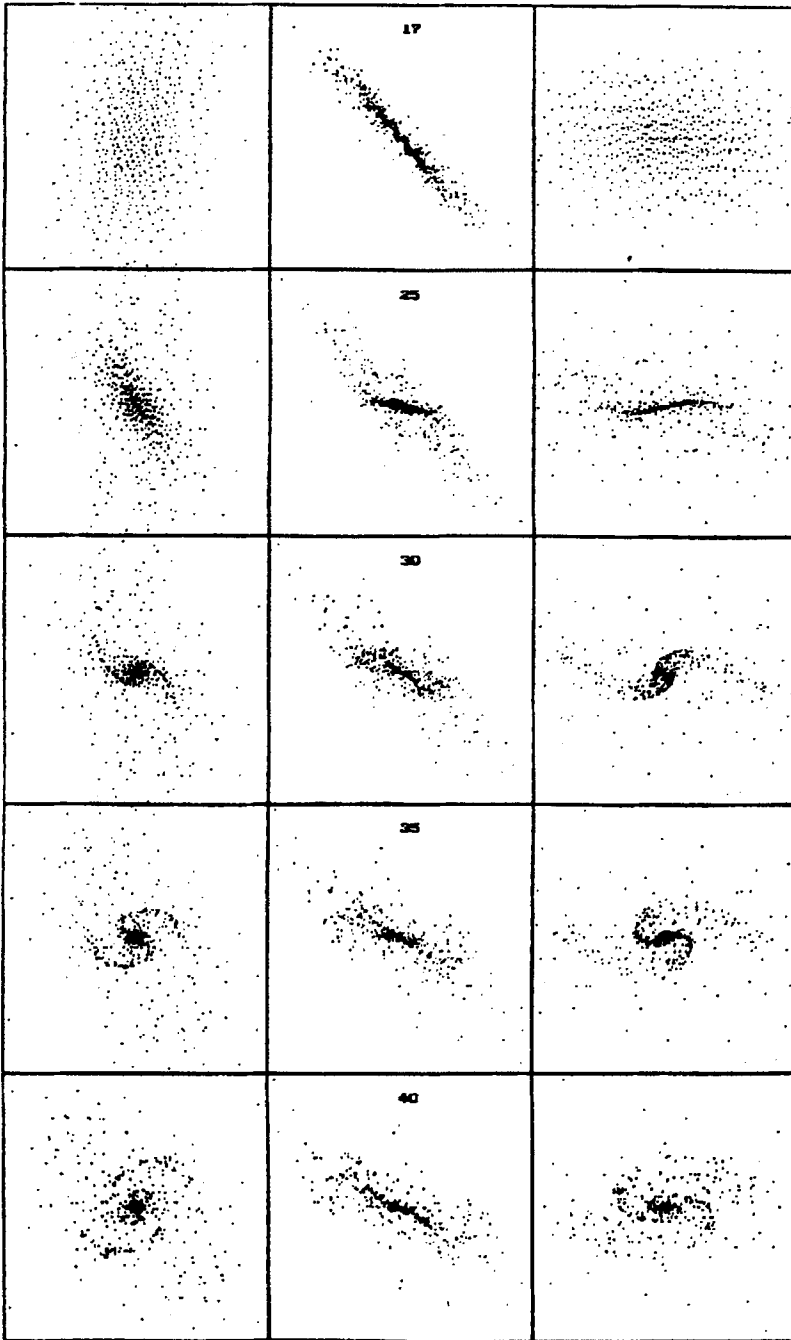
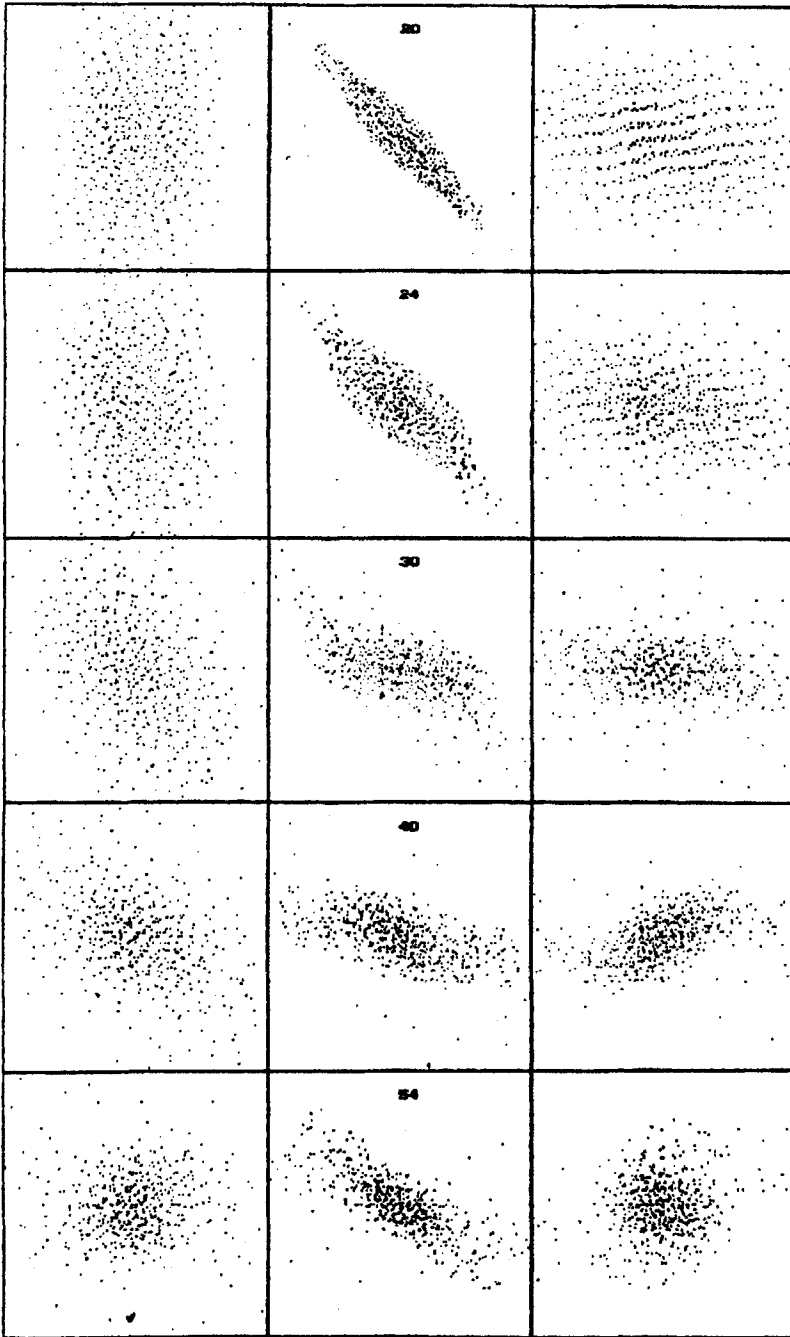


Figure 2 The model T1. The first column corresponds to XY plane; the second, XZ plane and the third, YZ plane. The step 14 corresponds to  $t \approx 0.46 \times 10^9$  year. The step 33 corresponds to  $t \approx 0.78 \times 10^9$  year. The diameter of the cell represented in the figure is 200 kpc.



**Figure 3** The model TT1. The first column corresponds to XY plane; the second, XZ plane and the third, YZ plane. The step 17 corresponds to  $t \approx 0.61 \times 10^9$  year. The step 40 corresponds to  $t \approx 1.07 \times 10^9$  year. The diameter of the cell represented in the figure is 200 kpc.



**Figure 4** The model TT1A. The first column corresponds to XY plane; the second, XZ plane and the third, YZ plane. The step 20 corresponds to  $t \approx 0.66 \times 10^9$  year. The step 54 corresponds to  $t \approx 1.67 \times 10^9$  year. The diameter of the cell represented in the figure is 200 kpc.

*The model B1.* The initial body of protogalaxy in model B1 is almost a disk structure. The  $A = 100$ ,  $B = 90$  and  $C = 50$  kpc. The initial angular momentum vector has only two components, the  $\Omega_{0x} = 0.8 \cdot \Omega_{\text{cir}}$  and  $\Omega_{0z} = 0.8 \cdot \Omega_{\text{cir}}$ . The initial temperature of gas is  $T_0 = 5 \times 10^5$  K. The initial density of a homogenous ellipsoid is  $\rho_0 \approx 0.015 \text{ cm}^{-3}$ . In all models to represent dynamical data we use the coordinate system in which the initial angular momentum have only one component  $\Omega_{0z}$ . The initial distribution of rotation velocity, in this coordinate system, is linear and has a maximum value  $V_{\text{rot}} \approx 250 \text{ km/s}$ .

The first step in Figure 1 corresponds to the time  $t \approx 0.61 \times 10^9$  year. During this time, the gas collapse along the rotation axes. This is shortest dynamical process. This process form a thin disk with complex velocity fields. The rotational velocity in the disk has a linear part (up to 50 kpc) and a flat one (the value of  $V_{\text{rot}} \approx 200 \text{ km/s}$ ). The velocity dispersion along the collapse axis has a maximum value  $V_z \approx 150 \text{ km/s}$ . The density in the disk has almost a power distribution with the maximum central value  $\rho_c \approx 0.8 \text{ cm}^{-3}$ .

The second step in Figure 1 corresponds to the time  $t \approx 0.75 \times 10^9$  year. At this time, we see an interesting collapse in the central part of a protogalaxy (up to  $\approx 20$  kpc) which form a thin, compact central disk. The rotational velocity in this disk is almost linear, with the maximum value near 20 kpc of  $V_{\text{rot}} \approx 400 \text{ km/s}$ . The velocity dispersion along the collapse axis has a maximum value  $V_z \approx 125 \text{ km/s}$ . The density in the central disk has a power distribution with the maximum central value  $\rho_c \approx 20 \text{ cm}^{-3}$ .

The third step in Figure 1 corresponds to the time  $t \approx 0.82 \times 10^9$  year. In this picture, we see a strong triaxial bar formation in the central regions with parameters typical for spiral galaxies.

In the Figure 5 we show a more detail view of step 35 in model B1. This step corresponds to  $t \approx 0.89 \times 10^9$  year. The diameter of the cell represented in the Figure 5 is 100 kpc.

The final stage in our calculations for this model corresponds to the time  $t \approx 0.98 \times 10^9$  year. At this step the central density already has a maximum value  $\rho_c \approx 300 \text{ cm}^{-3}$ . The rotation curve is typical for disk galaxies. It has a linear growing part up to 10 kpc and an extended flat tail up to 75 kpc. The maximum value of the rotation velocity is  $V_{\text{rot}} \approx 250 \text{ km/s}$ . After the flat tail we have a slowly dropping part of the rotation curve almost up to 140 kpc.

In Figure 6 we show the density distribution of the last step, the rotational velocity  $V_{\text{rot}}$  – in Figure 7 and the velocity distribution  $V_z$  (perpendicular to the plane of forming a galaxy) – in Figure 8.

Due to the body of protogalaxy not being symmetrical and rotating differentially, the collapse process generates the “warp” force that distors the disk and produce a spiral like structure. During the evolution this “warp” process generates an interesting spiral shape of the gas in the protogalaxy, especially in the central region (up to 20 kpc, see the Figure 5).

The model leads to the development of the triaxial central bar phenomenon. The bar have typical dimensions around 5 kpc. The model also shows the extended gas tail that have an essential inclination to the central disk. Therefore, we can

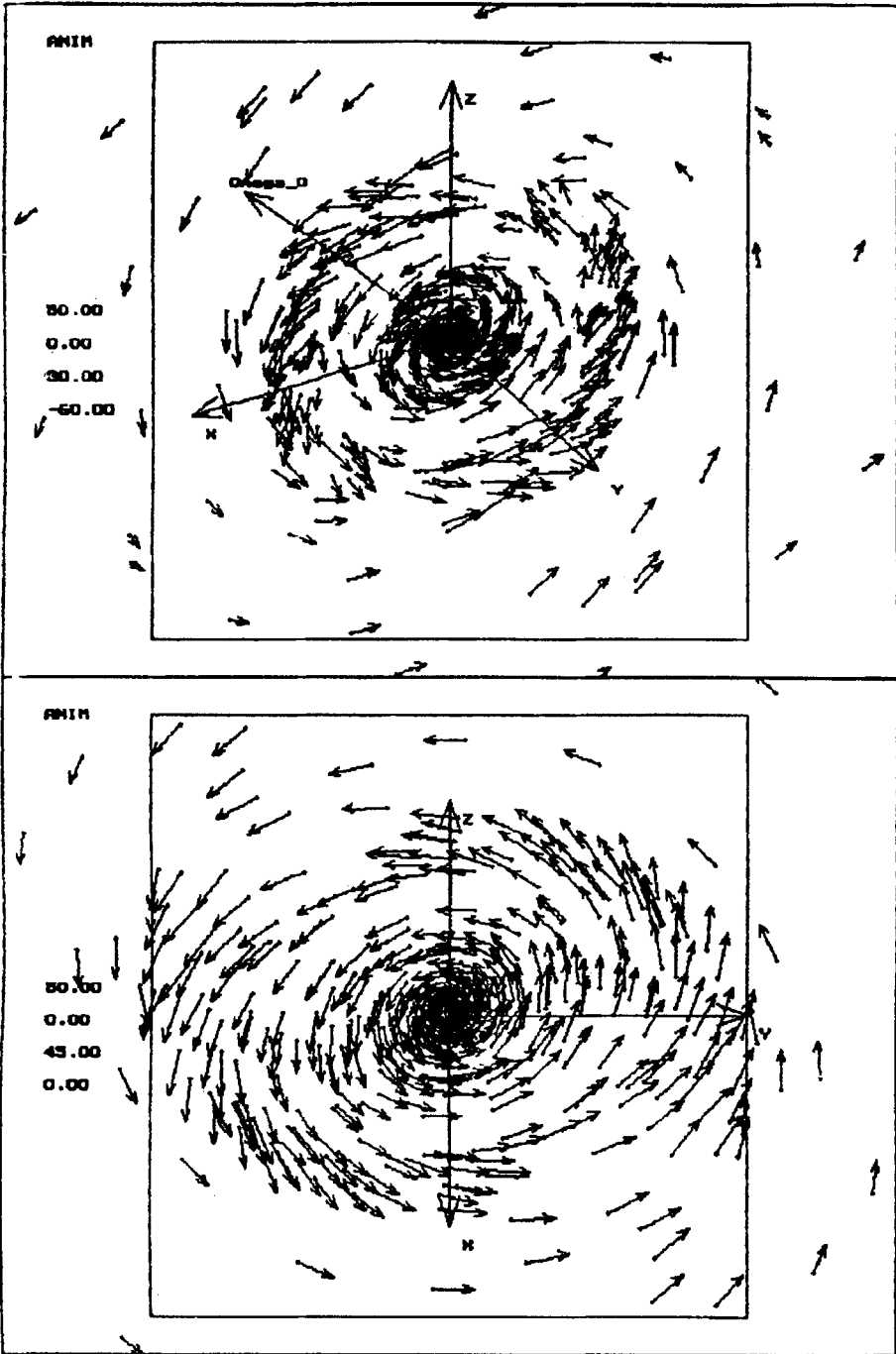


Figure 5 A more detail view of step 35 in model B1. This step corresponds to  $t \approx 0.89 \times 10^9$  year. The diameter of the cell represented in the figure is 100 kpc.

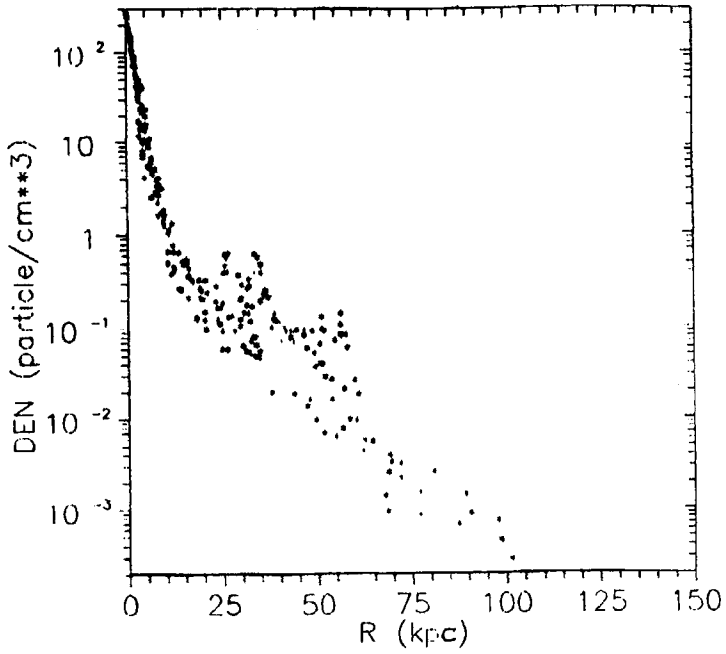


Figure 6 Density distribution of step 40 in model B1.

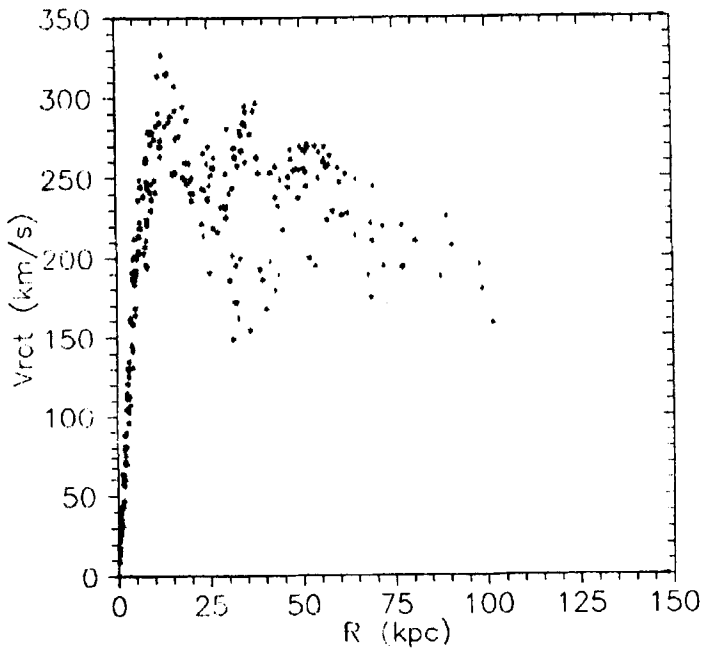
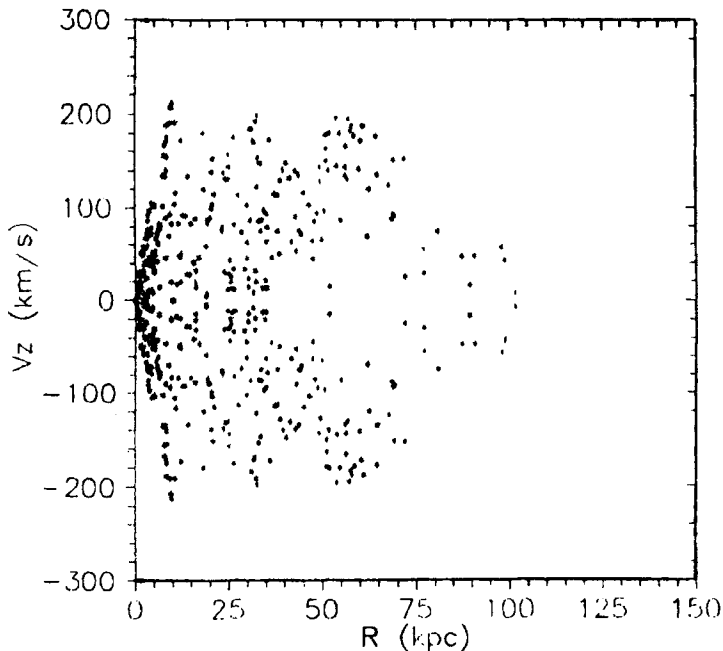


Figure 7 Rotational velocity  $V_{rot}$  of step 40 in model B1.



**Figure 8** Velocity distribution  $V_z$  (perpendicular to the plane of forming a galaxy) of step 40 in model B1.

observe in this case a complicated internal and external motion. The central part have a separate direction of rotation as compared with the external one forming a galaxy.

*The model T1.* The next model is T1. This model have almost a bar-like shape. The  $A = 100$ ,  $B = 60$  and  $C = 50$  kpc. The initial angular momentum vector has two components, the  $\Omega_{0x} = 0.5 \cdot \Omega_{\text{cir}}$  and  $\Omega_{0z} = 0.5 \cdot \Omega_{\text{cir}}$ . The initial temperature of gas, as in the model B1, is  $T_0 = 5 \times 10^5$  K. The initial density is  $\rho_0 \approx 0.023 \text{ cm}^{-3}$ . The initial distribution of the rotation velocity has a maximum value  $V_{\text{rot}} \approx 200 \text{ km/s}$ .

The first step in Figure 2 corresponds to the  $t \approx 0.46 \times 10^9$  year. This step, corresponds to the moment, when the collapse along the rotational axis is maximal. In the figure we see a strong elongated bar in the collapsed disk. The rotational velocity in the disk have a linear part (up to 30 kpc) and a wide flat one (the value of  $V_{\text{rot}} \approx 200 \text{ km/s}$ ). The velocity dispersion along the collapse axis has a maximum value  $V_z \approx 150 \text{ km/s}$ . The density in disk has a maximum central value  $\rho_c \approx 0.8 \text{ cm}^{-3}$ .

The second step in Figure 2 corresponds to the  $t \approx 0.58 \times 10^9$  year. At this time, we see the beginning of the process of generating a spiral perturbation in the central part of a protogalaxy (up to  $\approx 20$  kpc). The rotational velocity in the central disk is almost linear, with the maximum value of  $V_{\text{rot}} \approx 300 \text{ km/s}$  near 20 kpc. The



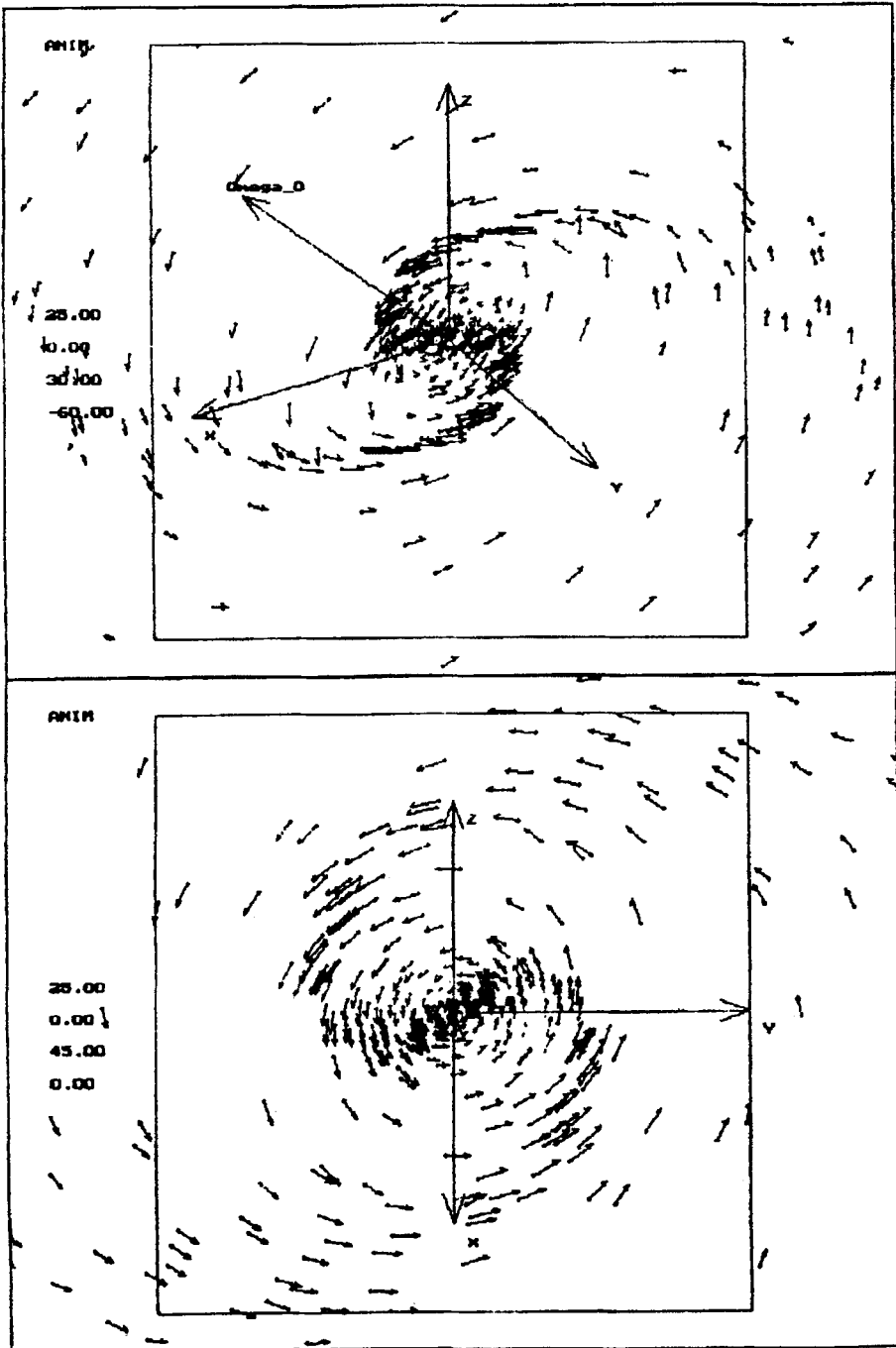


**Figure 9** A more detail view of step 25 in model T1. This step corresponds to  $t \approx 0.66 \times 10^9$  year. The diameter of the cell represented in the figure is 50 kpc.

velocity dispersion along the collapse axis has a maximum value  $V_z \approx 125$  km/s. The density in the central disk has a power distribution with the maximum central value  $\rho_c \approx 100$  cm $^{-3}$ .

The third step in Figure 2 corresponds to the  $t \approx 0.66 \times 10^9$  year. In this picture, we see a very impressive triaxial spiral shape formation in the central region of a protogalaxy. This spiral shape has parameters typical for spiral galaxies.

In Figure 9 we show a more detail view of step 25. The diameter of the cell represented in the Figure 9 is 50 kpc.

The final state of this model corresponds to the  $t \approx 0.78 \times 10^9$  year. In this step the central density has the value  $\rho_c \approx 500$  cm $^{-3}$ . In the central core the rotation curve is linear and has a maximum value  $V_{\text{rot}} \approx 300$  km/s. In the external part rotation curve is almost Keplerian.

Due to the initial rotation fields in this model being less than in the model B1, the final configuration is more compact and dense.

This model shows a very impressive bar instability and spiral pattern generation. The bar has dimensions, as in model B1, about 5 kpc. The spiral structure is very impressive but evolves very quickly.

*The model TT1.* The model TT1 have the most common triaxial shape. The  $A = 100$ ,  $B = 75$  and  $C = 50$  kpc. The initial angular momentum vector has two components,  $\Omega_{0x} = 0.8 \times \Omega_{\text{cir}}$  and  $\Omega_{0z} = 0.8 \times \Omega_{\text{cir}}$ . The initial temperature of gas is  $T_0 = 1 \times 10^5$  K. The initial density is  $\rho_0 \approx 0.018$  cm $^{-3}$ . The initial distribution of the rotation velocity has a maximum value  $V_{\text{rot}} \approx 250$  km/s.

The first step in Figure 3 is corresponds to the  $t \approx 0.61 \times 10^9$  year, the second step corresponds to the  $t \approx 0.80 \times 10^9$  year and the third step corresponds to the  $t \approx 0.88 \times 10^9$  year.

In the Figure 10 we show a more detail view of step 35 in model TT1. This step corresponds to  $t \approx 0.95 \times 10^9$  year. The diameter of the cell represented in the Figure 10 is 50 kpc.

The final state of the evolution, shown in the last step, corresponds to the  $t \approx 1.07 \times 10^9$  year. In this step the central density has a value  $\rho_c \approx 300$  cm $^{-3}$ . In the central core the rotation curve is linear and has a maximum value  $V_{\text{rot}} \approx 300$  km/s. In external part the velocity distribution shows a slowly falling trend.

The model produces a very nice spiral system. Two spiral arm extend beyond 20 kpc (see Figure 10).

*The model TT1A.* The model TT1A has the same initial conditions as TT1 but in this case we investigate an adiabatic evolution of a gas protogalaxy. The initial temperature of the gas is  $T_0 = 1 \times 10^4$  K.

The first step in Figure 4 corresponds to the  $t \approx 0.66 \times 10^9$  year, the second step corresponds to the  $t \approx 0.79 \times 10^9$  year and the third step corresponds to the  $t \approx 0.99 \times 10^9$  year.

The final state of evolution corresponds to the  $t \approx 1.61 \times 10^9$  year. In this step the distribution of density is very flat and corresponds to the power law, with the central density  $\rho_c \approx 0.2$  cm $^{-3}$ . In the central core (up to 50 kpc) the rotation curve is linear and has a maximum value  $V_{\text{rot}} \approx 200$  km/s. In external part the velocity distribution has a linear, slowly falling trend.

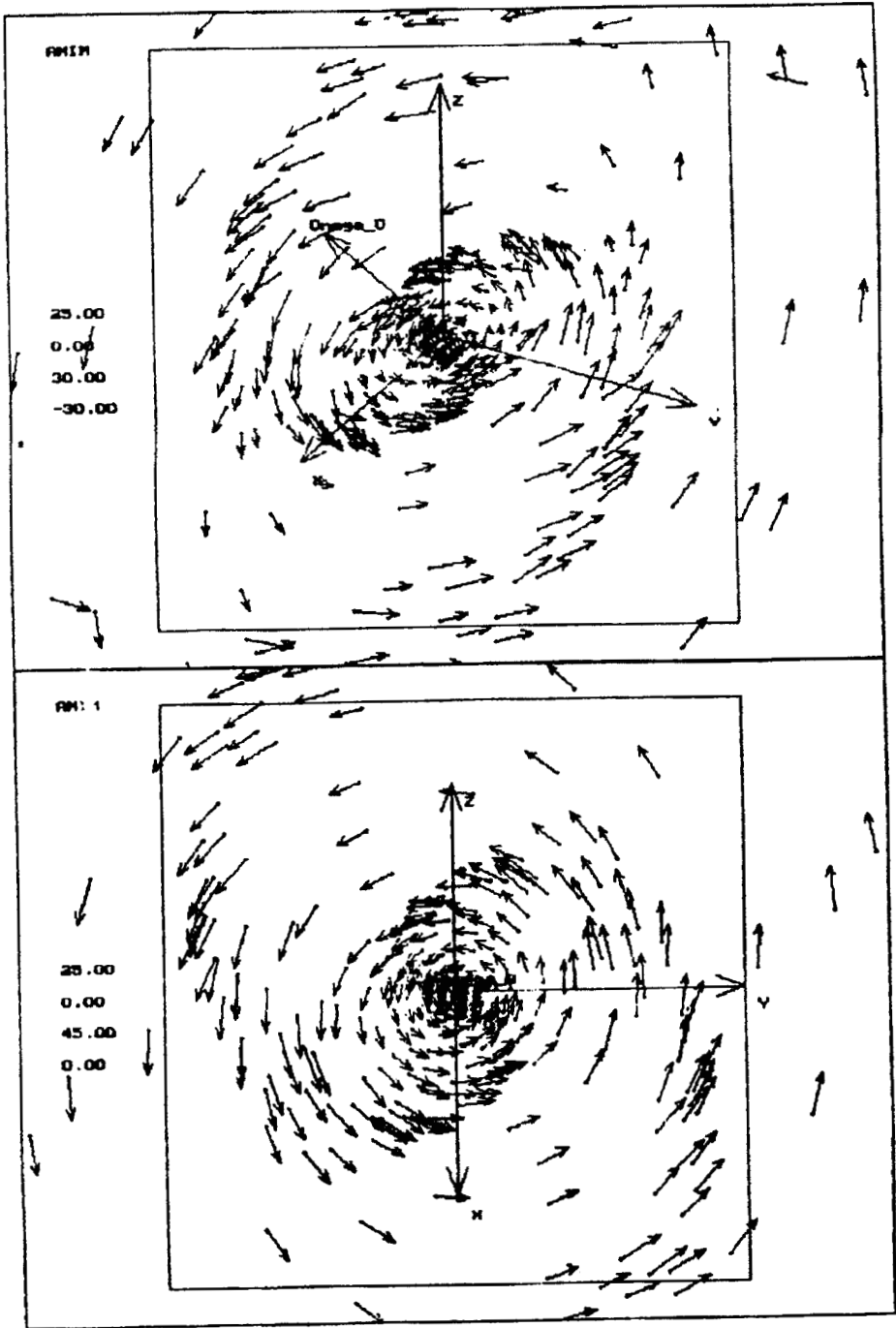


Figure 10 A more detail view of step 35 in model TT1. This step corresponds to  $t \approx 0.95 \times 10^9$  year. The diameter of the cell represented in the figure is 50 kpc.

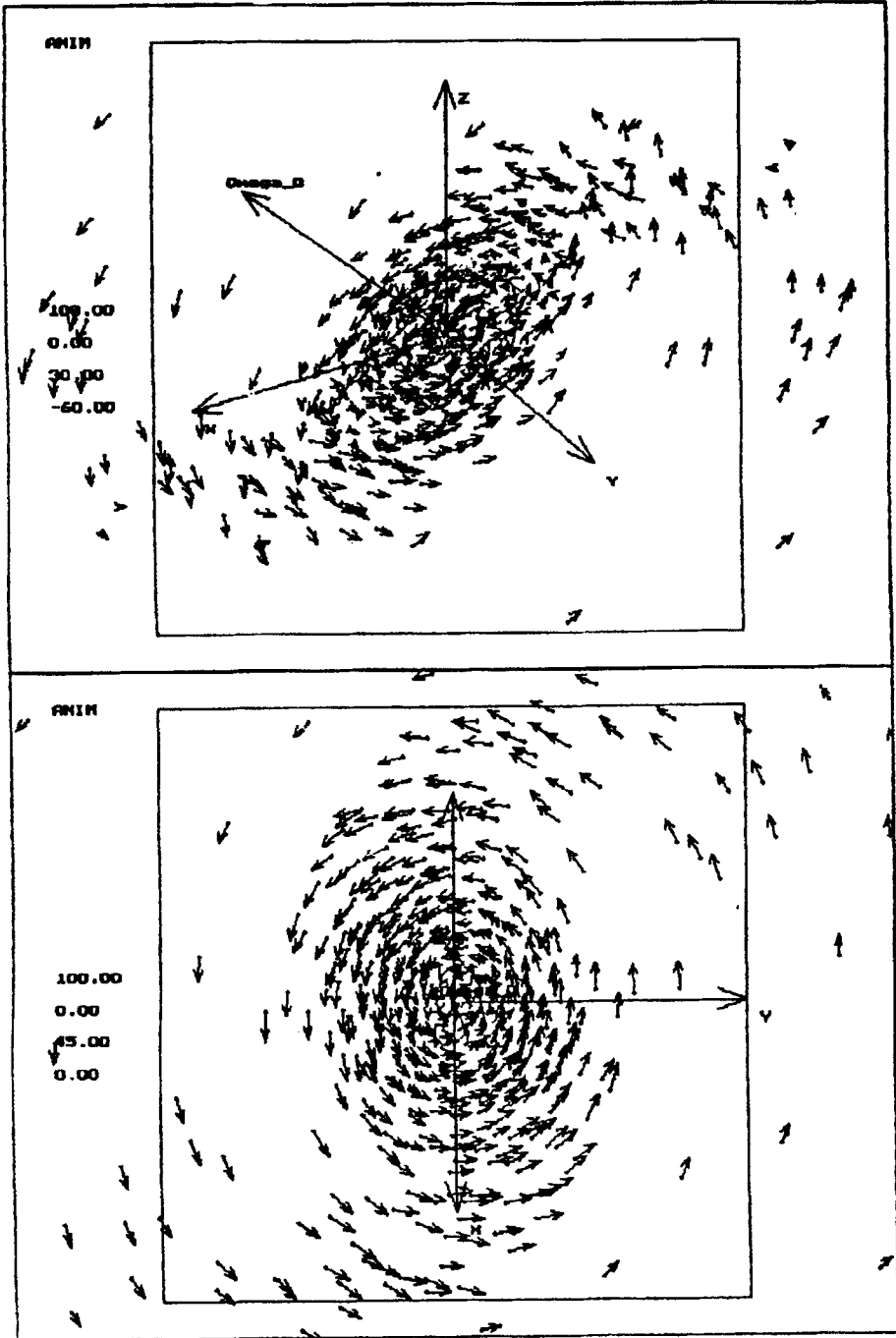


Figure 11 A more detail view of step 54 in model TT1A. This step corresponds to  $t \approx 1.61 \times 10^9$  year. The diameter of the cubic cell represented in the figure is 100 kpc.

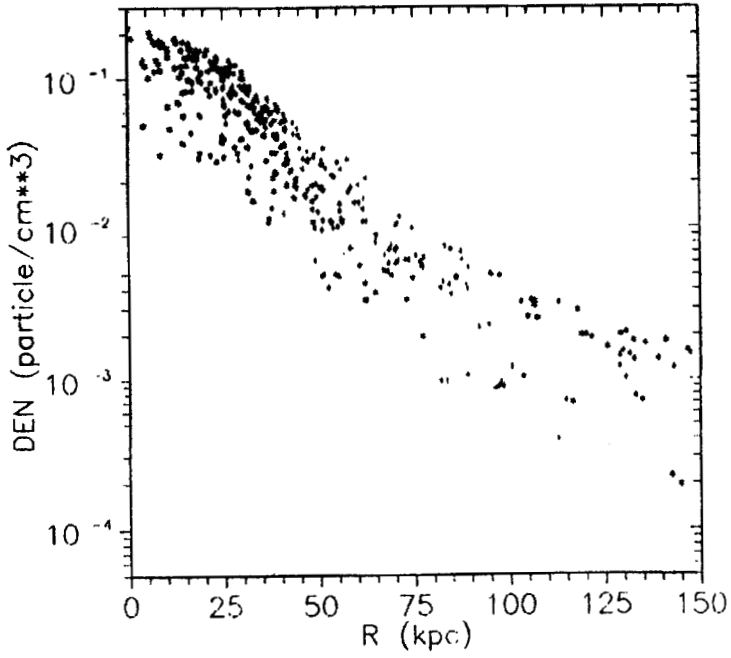


Figure 12 Density distribution of step 54 in model TT1A.

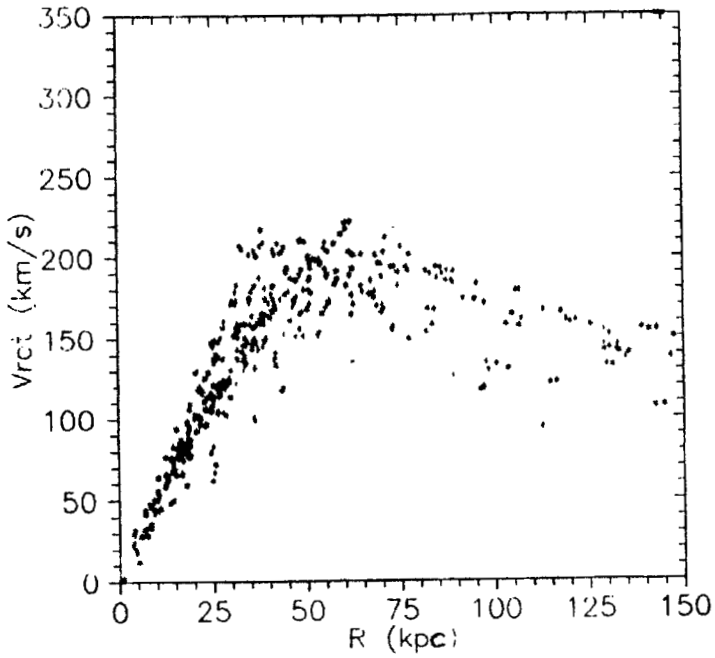


Figure 13 Rotational velocity  $V_{rot}$  of step 54 in model TT1A.

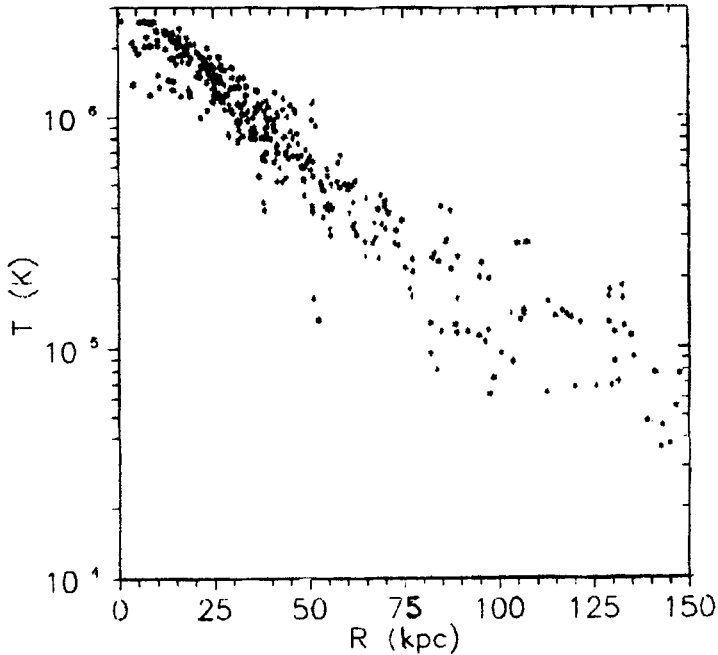


Figure 14 Temperature distribution  $T$  of step 54 in model TT1A.

In the Figure 11 we show a more detail view of the last step in model TT1A. The diameter of the cubic cell represented in the Figure 11 is 100 kpc.

In Figure 12 we show the density distribution of the last step, the rotational velocity  $V_{\text{rot}}$  - in Figure 13 and the temperature distribution  $T$  - in Figure 14.

This model demonstrates an interesting mechanism of bulge formation. The bulge has a triaxial form. It should be also noted that the kinematical properties of the central and peripheral part of the protogalaxy are definitely different (see Figure 11).

#### 4 CONCLUSIONS

In this paper, we describe a qualitative result of the properties of early, pure gas triaxial protogalaxies, which can be formed as a result of an isothermal or adiabatic collapse. We model the initial state of a protogalaxy as a homogeneous triaxial ellipsoid having an angular momentum arbitrarily oriented in space.

On the basis of the calculation model it follows that many interesting and complex properties of galaxies (such as the triaxial central bar phenomenon and inclined warp disk structures) may be explained using our suggestion about an initial triaxial shape and angular momentum direction in the early protogalaxy.

We may make several general conclusions about the early properties of forming protogalaxies:

- (1) In all cases the collapse in a triaxial model leads to forming a warp disk structure and an internal bar.
- (2) The dynamical evolution of the triaxial model generates a global spiral-like structure. In the isothermal model a spiral pattern is more sophisticated and long-lived.
- (3) The adiabatic phase of the collapse is important for a bulge formation and its parameters.
- (4) In the case of adiabatic models the kinematical properties of the core and peripheral parts of protogalactic clouds are extremely different.

### *Acknowledgments*

The authors are grateful to S. G. Kravchuk and L. S. Pilyugin for fruitful discussions during the process of preparing this work. P. Berczik would like to acknowledge the International Science Foundation for a partial financial support of this work under grant UC 9000 and UC 9200.

### *References*

- Aguilar, L. A. and Merritt, D. (1990) *Astrophys. J.* **354**, 33.  
 Berczik, P. P. and Kolesnik, I. G. (1993) *Kinematika i Fizika Nebesnykh Tel* **9**, No. 2, 3.  
 Berczik, P. P. and Kolesnik, I. G. (1995) In: Alfaro E. J., Delgado A. J. (eds.) *The Formation of the Milkyway*, Cambridge Univ. Press, 345.  
 Berdeen, J. M., Bond, J. R., Kaiser, N., and Szalay, A. S. (1986) *Astrophys. J.* **304**, 15.  
 Bertola, F., Vietori, M., and Zeilinger, W. W. (1991) *Astrophys. J.* **374**, L13.  
 Binney, J. (1978) *Mon. Not. Roy. Astron. Soc.* **183**, 501.  
 Binney, J. (1985) *Mon. Not. Roy. Astron. Soc.* **212**, 767.  
 Binney, J. (1992) *ARA and A* **30**, 51.  
 Blitz, L. and Spergel, D. N. (1991a) *Astrophys. J.* **370**, 205.  
 Blitz, L. and Spergel, D. N. (1991b) *Astrophys. J.* **379**, 631.  
 Chernin, A. D. (1993) *Astron. Astrophys.* **267**, 315.  
 Curir, A. and Diaferio, A. (1994) *Astron. Astrophys.* **285**, 389.  
 de Zeeuw, T. and Franx, M. (1991) *ARA and A* **29**, 239.  
 Eisenstein, D. J. and Loeb, A. (1995) *Astrophys. J.* **439**, 520.  
 Franx, M., Illingworth, G., and Heckman, T. (1989) *Astrophys. J.* **344**, 613.  
 Franx, M., Illingworth, G., and de Zeeuw, T. (1991) *Astrophys. J.* **383**, 112.  
 Hernquist, L. and Katz, N. (1989) *Astrophys. J. S.* **70**, 419.  
 Hiotelis, N., Voglis, N., and Contopoulos, G. (1991) *Astron. Astrophys.* **242**, 69.  
 Hiotelis, N. and Voglis, N. (1991) *Astron. Astrophys.* **243**, 333.  
 Illingworth, G. (1977) *Astrophys. J.* **218**, L43.  
 Kormendy, J. and Djorgovski, S. (1989) *ARA and A* **27**, 235.  
 Monaghan, J. J. (1992) *ARA and A* **30**, 543.  
 Monaghan, J. J. and Lattanzio, J. C. (1985) *Astron. Astrophys.* **149**, 135.  
 Peebles, P. J. E. (1969) *Astron. Astrophys.* **155**, 393.  
 Pfenniger, D. (1984) *Astron. Astrophys.* **134**, 373.

- Richter, O. G. and Sancisi, R. (1994) *Astron. Astrophys.* **290**, 9.  
Voglis, N. and Hiotelis, N. (1989) *Astron. Astrophys.* **218**, 1.  
Voglis, N. (1994) *Mon. Not. Roy. Astron. Soc.* **267**, 379.  
Weinberg, M. D. (1992) *Astrophys. J.* **384**, 81.  
White, S. D. M. and Silk, J. (1979) *Astrophys. J.* **231**, 1.  
Zurek, W. H., Quinn, P. J., and Salmon, J. K. (1988) *Astrophys. J.* **330**, 519.